ACS central science

http://pubs.acs.org/journal/acscii

Research Article

Slow Proton Transfer in Nanoconfined Water

Oleksandr O. Sofronov and Huib J. Bakker*

Cite This: https://dx.doi.org/10.1021/acscentsci.0c00340

Read Online

ACCESS | Metrics & More | Article Recommendations | Supporting Information

ABSTRACT: The transport of protons in nanoconfined environments, such as in nanochannels of biological or artificial proton conductive membranes, is essential to chemistry, biology, and nanotechnology. In water, proton diffusion occurs by hopping of protons between water molecules. This process involves the rearrangement of many hydrogen bonds and as such can be strongly affected by nanoconfinement. We study the vibrational and structural dynamics of hydrated protons in water nanodroplets stabilized by a cationic surfactant using polarization-resolved femtosecond infrared transient absorption spectroscopy. We determine the time scale of proton hopping in the center of the water nanodroplets from the dynamics of the anisotropy of the transient absorption signals. We find that in small nanodroplets with a diameter <4 nm, proton hopping is more than 10 times slower than in bulk water. Even in relatively large nanodroplets with a diameter of ∼7 nm, we find that the rate of proton hopping is slowed by ∼4 times compared with bulk water.

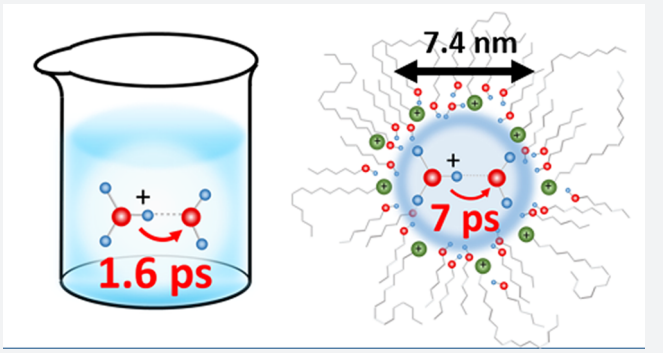

INTRODUCTION

Proton transfer in nanoconfined water is a process of paramount importance in biological and man-made systems, in particular in the generation and storage of energy.[1−4] Energy is stored in cells by proton transfer through the nanochannels of mitochondrial membranes, and the flow-back through these channels is coupled to the generation of ATP. In bulk liquid water, proton diffusion occurs through the so-called Grotthuss mechanism,[5] which implies that the proton does not move as a particle, but that rather its charge is being transferred between hydrogen atoms located on different water molecules.

In several theoretical studies, it was found that the transfer of the proton charge in liquid water results from the interconversion between $H_9O_4^+$ Eigen proton-hydration structures located at different positions in the liquid, with Zundel $H_5O_2^+$ proton hydration structures acting as short-living intermediates.[6−9] However, recent *ab initio* molecular dynamics (AIMD) simulations of the vibrational spectrum of acid water indicated that the Zundel species is in fact quite prominently present in acid water.[10−13] This notion was confirmed in a two-dimensional infrared spectroscopy study by Fournier et al.,[14] in which it was shown that the proton in aqueous solution forms a single spectroscopically distinct species, which can best be described as an asymmetric Zundel structure.

Proton transfer in liquid water is intimately connected to the reorganization of the hydrogen-bonded network of the water solvent. As the properties of water in nanoconfinement such as the polarity and self-diffusion are different from bulk,[15,16] it is to be expected that nanoconfinement of the water matrix will strongly affect the rate and mechanism of aqueous proton transfer. Very suitable systems to study the effect of nanoconfinement on the dynamics of water and aqueous protons are reverse micelles: water nanodroplets in an apolar matrix that are stabilized by surfactant molecules with a polar head and an apolar tail. The diameter of the water nanodroplet (d_w) can often be varied over a quite large range by varying the hydration ratio $w_0 = [H_2O]/[surfactant]$. Reverse micelles have thus been used to study the effect of nanoconfinement on the release and solvation of protons by photoacid molecules.[17−21] In these studies it was found that the proton release occurs much slower in nanoconfined water than in bulk. These results indicate that nanoconfinement strongly affects aqueous proton transfer. Unfortunately, a detailed understanding of the effect of nanoconfinement on proton transfer in these studies is complicated by the fact that the observed proton-release dynamics also rely on the water solvation dynamics of a relatively large conjugate photobase and that the photoacid molecules are often not uniformly distributed over the water nanodroplet.[22]

The anionic Aerosol OT (dioctyl sulfosuccinate, AOT) is an ideal surfactant to create reverse micelles over a wide range of sizes. AOT reverse micelles have thus been widely used to

Received: March 23, 2020

study the effect of nanoconfinement on the dynamics of liquid water.[23−25] For the study of nanoconfinement on aqueous proton transfer, AOT reverse micelles are less suitable because the protons will strongly interact with the negatively charged sulfonate groups of the surfactant molecules.[26−28]

Here we study the vibrational and structural dynamics of hydrated protons in water nanodroplets of cationic reverse micelles using polarization-resolved femtosecond infrared (fs-IR) transient absorption spectroscopy. We use a positively charged surfactant system consisting of CTAB (cetyltrimethylammonium bromide) and hexanol, where the addition of hexanol as a cosurfactant allows to prepare much more stable and monodisperse nanodroplets.[29,30] Recent small-angle neutron scattering (SANS) studies[29] showed that water nanodroplets stabilized by these surfactants in an apolar solvent have an ellipsoid shape with an axial ratio between 1.7 for small nanodroplets (w_0 < 17) and 1.1−1.3 for large nanodroplets (w_0 > 20). Since the shape is near-spherical, we will further use the diameter d_w of a sphere of equal volume to refer to the size of the studied nanodroplet (for details, see the Methods section). In microemulsions, the reverse micelles move and collide, which can result in intermicellar exchange. However, these processes take place on a much slower time scale (typically microseconds) than the time frame of our experiments (picoseconds). Hence, in our experiment, the emulsion of reverse micelles can be considered to be a static system.

In cationic reverse micelles, excess protons will not bind to the positively charged surfactants, which implies that the protons will be well embedded and hydrated in the core of the nanodroplet. We can thus measure the "pure" effect of nanoconfinement, with very little influence of the surface of the nanoconfined region. We observe that nanoconfinement leads to a very strong slowing down effect on the rate of aqueous proton transfer. Even for relatively large nanodroplets with a water pool diameter of 7.4 nm, proton transfer occurs ∼4 times slower than in bulk water.

RESULTS

In Figure 1A, we show Fourier transform infrared (FTIR) absorption spectra of neat water nanodroplets and nanodroplets containing a 7 M HBr solution. We vary the ratio $w_0 = [H_2O]/[surfactant]$ between w_0 = 12 and w_0 = 40, corresponding to a variation in nanodroplet diameter of 2.2−7.4 nm (see Methods). The presence of excess protons in the nanodroplets is observed to yield a broad continuous absorption at frequencies below 2800 cm^{-1}, similarly as has been observed for bulk liquid water. The broad featureless absorption at 2000−3000 cm^{-1} has been assigned to the OH-stretch vibrations of different proton hydration structures, whereas the absorption band observed at 1750 cm^{-1} is usually assigned to the bending vibrations of these structures.[31−33]

In Figure 1B, we zoom in on the absorption continuum of the hydrated proton OH-stretch vibrations. The spectrum is nearly flat below 2500 cm^{-1} and increases in amplitude for frequencies above 2500 cm^{-1}. The absorption spectrum of the nanodroplets is quite similar to the absorption spectrum of bulk acid water.

To study the dynamics of the hydrated proton we measure transient absorption spectra following the excitation of the proton OH-stretch continuum with an intense 100 fs infrared pulse centered at 2600 cm^{-1}. Figure 2A shows the resulting isotropic transient absorption spectra of hydrated protons in d_w

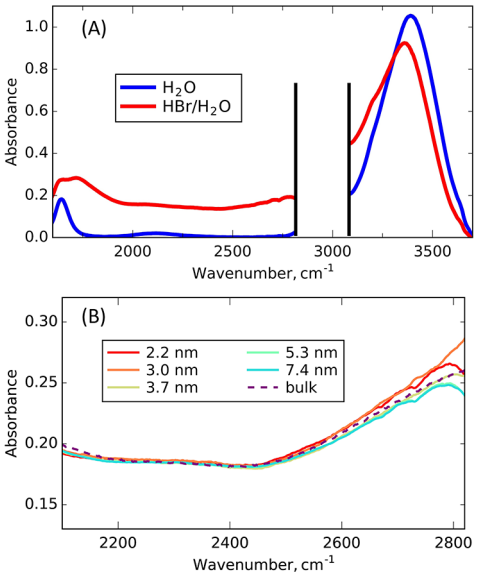

Figure 1. (A) Linear infrared absorption spectrum of the water nanodroplets (d_w = 2.2 nm) with (red) and without (blue) protons. The 2800−3100 cm^{-1} spectral region is not accessible because of the strong absorption of CH-stretch vibrations. (B) Comparison of the OH-stretch continuous absorption of the hydrated proton in nanodroplets of different diameters and in bulk water. In these spectra, the neat water contribution is subtracted.

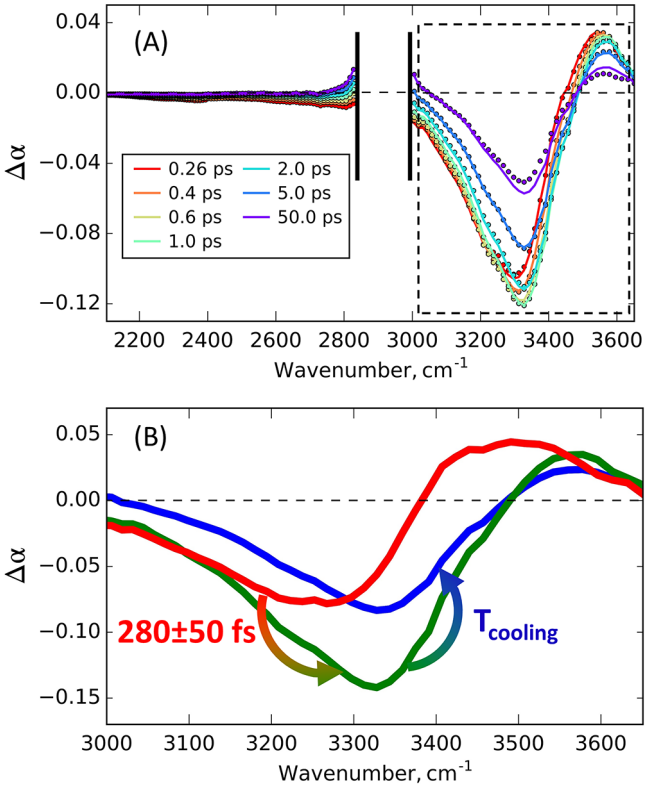

Figure 2. (A) Isotropic transient spectra of the acid water (7 M HBr) nanodroplets (d_w = 2.2 nm) following excitation at 2600 cm^{-1}. The lines are the result of the fit. The dashed box highlights the part of the spectrum that corresponds to the response of water molecules in the outer hydration shells of the proton. (B) Spectral components obtained from the fit of the transient spectral dynamics.

https://dx.doi.org/10.1021/acscentsci.0c00340
ACS Cent. Sci. XXXX, XXX, XXX−XXX

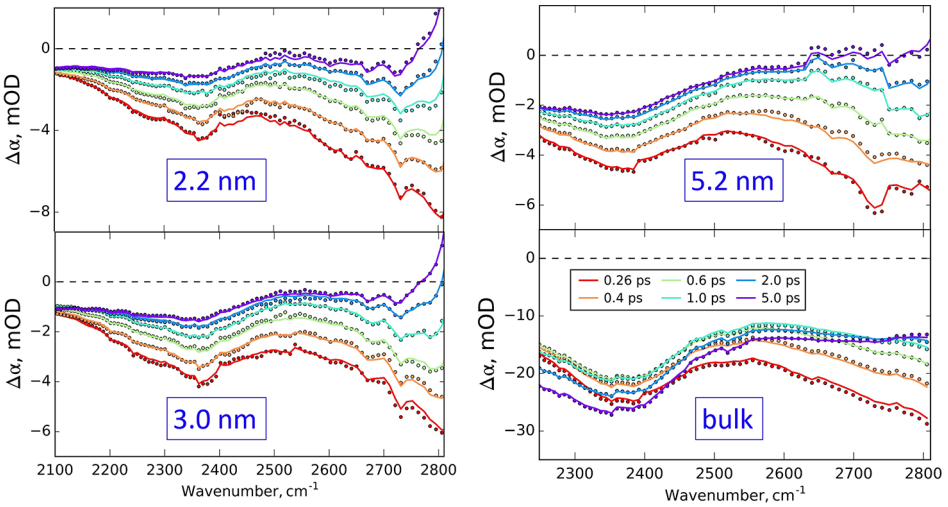

Figure 3. Isotropic transient spectra of acidic CTAB reverse micelles of different diameters and a bulk solution of HBr (7 M) in water following excitation at 2600 cm^{-1}. The lines are the result of a fit of the kinetic model described in the text.

= 2.2 nm nanodroplets at different time delays between the excitation and detection pulses, ranging from 0.26 to 5 ps. At all delay times, the spectra consist of a weak and broad negative signal below 2800 cm^{-1}, a much more intense negative signal centered at ∼3300 cm^{-1}, and a positive absorption change above 3500 cm^{-1}. This shape of the transient absorption spectrum is observed for all studied nanodroplet sizes (Figures S1, S2). The 2800−3000 cm^{-1} region is not accessible due to the high absorbance of the alkyl chains of the surfactant molecules.

First, we focus on the high-frequency part of the transient spectrum (highlighted in Figure 2A, Figure S3). The observed strong negative absorption change and smaller positive absorption change at higher frequency is a typical signature of the hot ground state of the OH-stretch vibration of water that results from the transfer of vibrational energy to low-frequency degrees of freedoms (e.g., hydrogen bonds) following the relaxation of the excited OH stretch vibration.[34−36] This process results in a blue shift of the OH-stretch absorption spectrum, which is similar to the effect of increasing the temperature of the sample.[37]

In the first picosecond after the excitation, the hot ground-state spectrum grows in amplitude and shifts to higher frequency. After 1 ps the signal slowly decays reaching a constant level after ∼50 ps. We fit these spectral dynamics with a cascade kinetic model consisting of three states. From the fit, we obtain the spectral components shown in Figure 2B. The first state has a red-shifted transient spectrum with a minimum at ∼3200 cm^{-1} and decays with a time constant of 280 ± 50 fs to the second state. The second state has a transient spectrum with a minimum at ∼3300 cm^{-1} and slowly decays to the third state with a transient spectrum of similar shape but with a reduced amplitude. The time constant of the latter relaxation process depends on the nanodroplet size.

A pump pulse centered at 2600 cm^{-1} cannot excite water OH-stretch vibrations near 3300 cm^{-1}. The observed early time transient spectral response near 3300 cm^{-1} (red spectrum in Figure 2B) is thus the result of ultrafast energy relaxation of the initially excited OH stretch vibration of hydrated protons, leading to heating of water molecules that are close to the excited OH stretch vibration. These water molecules are close to the positive proton charge and thus will have relatively strong hydrogen bonds and a red-shifted absorption spectrum compared to water molecules in bulk liquid water. The subsequent transition from the red to the green transient spectrum can be assigned to energy transfer from water molecules close to the initially excited core of the hydrated proton, to water molecules further away. These latter water molecules will have weaker hydrogen bonds and thus a more blueshifted absorption spectrum. The final slow decay of the green to the blue transient spectrum corresponds to the dissipation of the heat to surfactant molecules and the oil phase (i.e., cooling of the water nanodroplet). This process leads to a decrease of the amplitude of the transient absorption spectrum. The dynamics of this latter process are non-exponential and depend on the nanodroplet diameter.[38,39]

In Figure 3, we show transient absorption spectra at frequencies <2800 cm^{-1} for different nanodroplet sizes. This part of the spectrum corresponds to the OH-stretch vibrations of the core of the proton hydration structures, that is, OH-vibrations for which the H atom carries a significant fraction of the excess positive proton charge.[40]

Since at very short delay times we already observe a strong heating signal from water molecules (Figure 2), we conclude that excited OH-stretch vibrations at 2600 cm^{-1} relax ultrafast within the time resolution (∼100 fs) of the experiment. This means that the transient spectra at frequencies <2800 cm^{-1} are not due to the population of the excited $v = 1$ state of the OH vibrations but rather reflect a local heating effect on the absorption spectrum of the proton hydration structure.

The spectral dynamics are observed to be nonexponential, showing a fast and a slow processes. We fit these dynamics with the same three-level model used to fit the high frequency part of the spectrum shown in Figure 2. The first decay with a time constant of 280 ± 50 fs again reflects the energy equilibration with the proton hydration structure and the second much slower decay the cooling of the whole nanodroplet.

The amplitude of the transient absorption spectra increases for frequencies >2500 cm^{-1}, an effect that is also observed in the linear infrared absorption spectra (Figure 1B). Interestingly, the lower-frequency region of the transient spectra is not as featureless as the corresponding frequency region in the linear absorption spectrum. The transient absorption spectra

https://dx.doi.org/10.1021/acscentsci.0c00340
ACS Cent. Sci. XXXX, XXX, XXX−XXX

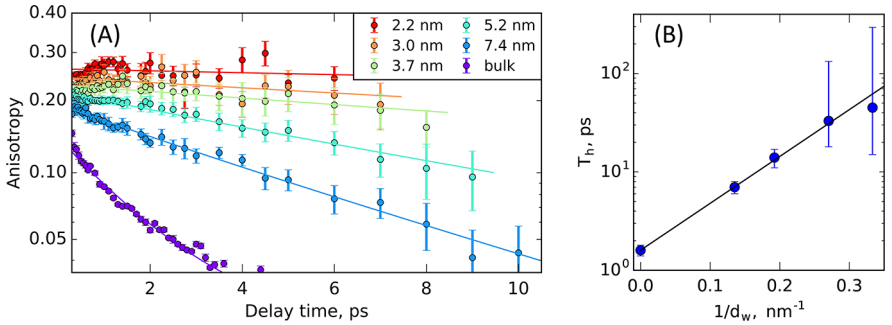

Figure 4. (A) Anisotropy of the transient signal at 2600 cm^{-1} as a function of delay time for acidic CTAB reverse micelles of different sizes and a bulk HBr (7 M) solution, plotted on a logarithmic scale. The straight lines represent exponential fits to the anisotropy decays. (B) Proton hopping time extracted from anisotropy dynamics as a function of the inverse water nanodroplet diameter. The straight solid line serves as a guide to the eye.

show a distinct band at 2350 cm^{-1} region. This band is not the result of nanoconfinement, as it is also present in the transient spectrum of the hydrated proton in bulk liquid water.

The response of the hydrated proton is anisotropic: the absorption change measured with a probe pulse that is polarized parallel to the polarization of the pump is larger than the absorption change measured with a probe pulse that has a perpendicular polarization. To quantify these observations we calculate the anisotropy value, which is the normalized difference between the absorption changes in parallel and perpendicular polarizations (see Methods section).

In Figure 4A, we show the anisotropy dynamics of the transient absorption signal at 2600 cm^{-1} following excitation with a pump pulse centered at 2600 cm^{-1}, for acidic water nanodroplets of different sizes and for acidic bulk water. The corresponding transient absorption signals measured in parallel and perpendicular polarization configuration are shown in Figure S4. The dynamics of the anisotropy of the signal measured with the same excitation and detection frequencies represents the reorientation of the transition dipole moments of vibrations absorbing at that frequency.

For bulk water, we observe a decay of the anisotropy with a time constant of 1.6 ± 0.2 ps, which is in excellent agreement with the proton hopping time derived from NMR experiments[41] (see also Supporting Information, Figure S5). The anisotropy decay is much slower for the nanodroplets and strongly slows down with decreasing size of the nanodroplet. For the smallest nanodroplets (d_w = 2.2 nm), the anisotropy does not decay at all within the accessible time window. For this nanodroplet size, even a small rise of the anisotropy is observed, which we can explain from the contribution of protonated hexanol molecules that have a slightly higher anisotropy and of which the transient absorption signal decays somewhat slower than that of hydrated protons (see Supporting Information, Figures S6, S7). For the larger nanodroplets ($d_w \geq$ 3.0 nm), the contribution of protonated hexanol is too small to significantly affect the anisotropy dynamics. For the large nanodroplets (5.2 and 7.4 nm), we extracted effective decay times of anisotropy of 13 ± 3 ps and 7 ± 1 ps, respectively. In Figure 4B, we present the anisotropy decay time constant as a function of the inverse nanodroplet diameter.

DISCUSSION

The anisotropy represents the average relative orientation of the transition dipole moment of the probed vibration with respect to the transition dipole moment of the excited vibration. For a single, well-localized vibration the initial value R_0 of the anisotropy is expected to be 0.4. When the absorption bands of strongly coupled vibrations with different orientation of their transition dipole moment overlap, the anisotropy rapidly decays, often even within the time resolution of the experiment. This is for instance observed for the symmetric and antisymmetric OH-stretch vibrations of water molecules in acetonitrile.[42] In the case of rapid randomization of the vibrational excitation in a planar symmetric molecular structure like the H_3O^+ cation, the value of R_0 is thus expected to be 0.1. The initial value of anisotropy R_0 can thus be interpreted as the level of degeneracy of the vibration. The observed R_0 values of 0.2−0.25 (Figure 4A) are below 0.4, which indicates, that the OH-stretch vibrations of the hydrated proton have a certain degree of degeneracy. These values are also higher than 0.1, which indicates that the probed OH-vibrations are more restricted in orientation than in an ideal planar symmetric H_3O^+. Thus, in line with previous experimental[14] and theoretical[6−8] works, we conclude that the proton hydration structure can be described as an asymmetric Eigen or Zundel structure.

The decay of the anisotropy reflects the randomization of the orientation of the transition dipole moment of the probed vibration. In the measurements of Figure 4A, the anisotropy is due to a local heating effect on the O−H stretch vibrations absorbing at 2600 cm^{-1}. This anisotropy can potentially decay as a result of three different processes: (1) diffusion of the locally dissipated heat to other proton hydration structures that were not excited and that have OH vibrations absorbing at 2600 cm^{-1} with a random orientation; (2) molecular rotation of the OH groups of the hydrated proton structure absorbing at 2600 cm^{-1}; (3) structural reorganization of the proton hydration structure as a result of which other, nearby O−H stretch vibrations with different orientations acquire absorption at 2600 cm^{-1}. This latter process would imply a transfer of the proton charge to another position in the liquid (i.e., a proton jump).

Heat diffusion does not require a restructuring of the hydrogen bonds of the proton hydration structure. For the hydration shells of hydroxide ions, it was found that heat diffusion constituted the dominant mechanism, leading to decay of the anisotropy of the signal of the hydration shell of the hydroxide.[43] The importance of heat diffusion was evident from the fact that the rate of anisotropy decay was observed to increase with increasing hydroxide concentration (i.e., decreasing average distance between the hydroxide solvation complexes). We find that for bulk acid solutions, the

https://dx.doi.org/10.1021/acscentsci.0c00340
ACS Cent. Sci. XXXX, XXX, XXX−XXX

anisotropy dynamics does not depend on the proton concentration (see Supporting Information, Figure S5), which shows that heat diffusion does not form a significant contribution to the decay of the anisotropy. This finding agrees with the results of a previous study by Carpenter et al.[44] of the anisotropy dynamics of hydrated protons in bulk water. It should also be noted that the global thermalization of the excitation energy (second relaxation process), that is the result of heat diffusion, leads to a nearly zero transient absorption signal at 2600 cm^{-1} (Figure 3). This means that for the nanodroplets the signal resulting from heat diffusion forms a negligible (isotropic) contribution to the observed total transient absorption signal at 2600 cm^{-1}. Hence, heat diffusion leads to a decay of the total transient absorption signal at 2600 cm^{-1}, but as this decay leads to an almost complete vanishing of the transient absorption signal, it will have very little effect on the dynamics of the anisotropy of the remaining signal at 2600 cm^{-1}.

In bulk liquid water, the molecular reorientation of OH groups occurs with a time constant of ∼2.5 ps.[45,46] This reorientation involves a reorganization of the hydrogen-bond network as a result of which the hydrogen bond of the probed OH group is broken and transferred via an intermediate state consisting of a bifurcated hydrogen bond to a hydrogen bond to another water molecule. For strongly hydrogen-bonded OH groups absorbing at 2600 cm^{-1}, this process is expected to be much slower than for the OH groups in bulk liquid water. It should further be noted that reorientation of the originally excited OH group at 2600 cm^{-1} results in a new hydrogen-bonded structure in which the rotated OH group likely absorbs at a different (higher) frequency and in which other OH groups acquire absorption at 2600 cm^{-1}. In this case, molecular reorientation is the same process as structural reorganization of the hydrogen-bond network in which the absorption at 2600 cm^{-1} is transferred to OH stretch vibrations different from the originally excited OH stretch vibration.

The reorganization of the hydrogen-bond structure can thus lead to proton transfer and a decay of the anisotropy. A prerequisite for the latter is that the net orientation of the new OH stretch vibrations absorbing at 2600 cm^{-1} differs from the orientation of the excited OH group. These new OH stretch vibrations are the water-like OH groups that before the hydrogen-bond reorganization absorb at frequencies 3000−3700 cm^{-1} (Figure 2) and that are directly affected by the vibrational energy relaxation and dissipation of the excited OH stretch vibration at 2600 cm^{-1}. We observe the anisotropy of the transient absorption signal of these OH groups to be zero (Figure S3), which means that these OH groups have no net orientation with respect to the excited OH vibration at 2600 cm^{-1}. Hence, irreversible transfer of the proton charge to other, nearby OH groups will convert the initial anisotropic signal at 2600 cm^{-1} into an isotropic signal at this frequency and thus will lead to a decay of anisotropy.

The assignment of the anisotropy decay to the structural reorganization of the hydrogen-bond network, leading to irreversible proton transfer, agrees with the results of a recent fs-IR spectroscopy study by Carpenter et al.[44] In this latter study, the transient signal of the OH-bending vibration of proton hydration structures following its excitation at 1750 cm^{-1} was measured. The observed anisotropy dynamics yielded an upper limit for the proton hopping time of 2−2.5 ps. This time constant agrees quite well with the time constant of 1.6 ± 0.2 ps that we observe for the decay of the anisotropy for bulk water and is consistent with previous experimental and theoretical works.[5,47,48] An experimental difference with the study of Carpenter et al.[44] is that we measure the anisotropy dynamics of the response of the OH-stretch vibrations of the hydrated protons. This has as an advantage that the observed transient absorption response does not show any contribution of ordinary water molecules, as the OH vibrations of these molecules absorb at frequencies >2900 cm^{-1}. For the bending region, there is not such a clear separation of the bending modes of the proton hydration structures (centered at 1750 cm^{-1}) and water molecules (centered at 1650 cm^{-1}).

For the 5.2 and 7.4 nm nanodroplets, we extracted the decay times of the anisotropy of 13 ± 3 ps and 7 ± 1 ps, respectively. Thus, even in large nanodroplets with a water pool diameter d_w = 7.4 nm, the proton hopping occurs ∼4 times slower than in bulk water. We observe a clear increase of the proton hopping time when decreasing the nanodroplet diameter (Figure 4B); however, the uncertainty of the values for d_w < 4 nm does not allow us to quantify this dependence. The lack of decay of the anisotropy of the smaller nanodroplets (d_w = 2.2 nm; 3.0 nm) in our time window of ∼6 ps, shows that for these water nanodroplets, the proton transfer is slowed by more than a factor of 10 in comparison to bulk liquid water. This slowing down of proton transfer in nanoconfined water is in qualitative agreement with the results of previous studies of photoacid dissociation in reverse micelles that were stabilized with anionic (AOT = sodium dioctyl sulfosuccinate) and nonionic (BRIJ-30 = polyoxyethylene(4)lauryl ether) surfactants. In these studies, a strong slowing down of the proton release with decreasing nanodroplet size was observed.[17−21] However, the strong dependence of the photodissociation on the dynamics of solvation of the photoacid and the conjugated base does not allow for a quantitative comparison of these results to the proton hopping dynamics studied here.

The effect of nanoconfinement on the proton transfer rate depends on the dimensionality of the nanoconfinement. Recent studies of proton transfer in water nanotubes[49,50] (two-dimensional confinement) and water layers[51] (one-dimensional confinement) showed that the proton mobility is not very different from bulk water in the dimensions that are not confined. Apparently, the fact that the hydrogen-bond network of water is still extended in one or two dimensions allows for a relatively high mobility of the proton in those dimensions. In the case of water nanodroplets (three-dimensional confinement), the proton can only move in dimensions that are confined, and the effect on the proton mobility in these dimensions is much higher than in the unconfined dimensions of water layers and water nanochannels.

An interesting question is how the observed strong decrease of the proton transfer rate upon three-dimensional nanoconfinement in CTAB reverse micelles can be explained. This slowing down cannot be explained from surface effects. It was shown with small-angle neutron scattering (SANS) experiments that the shape of the studied nanodroplets is nearly spherical or only slightly ellipsoidal.[29] For such a shape, only a small part of the water molecules will be in close contact with the surface effects (∼20% of the volume for a droplet with a diameter of 7.4 nm). The limited effect of the surface is further confirmed by the low fraction of water molecules showing a slower vibrational relaxation as a result of their location near the surface of the reverse micelle (see Supporting Information).

https://dx.doi.org/10.1021/acscentsci.0c00340
ACS Cent. Sci. XXXX, XXX, XXX−XXX

The strong slowing down of the proton transfer can also not be explained from ordering of water molecules by the field of the electric double layer at the charged surface of the nanodroplets. Vibrational sum-frequency generation experiments have shown that the effect of water ordering near charged surfaces is strongly suppressed for salt solutions.[52−54] Already at a bulk concentration of 0.5 M NaBr, the ordering of water near a CTAB monolayer is suppressed by an order of magnitude.[52] Thus, having an even higher ionic strength in the HBr containing reverse micelles, we do not expect significant ordering of water molecules beyond one molecular layer from the interface. This notion is confirmed by molecular dynamics simulations of nanodroplets stabilized by charged surfactants, which show that the fraction of water molecules whose motion is restricted by the electric dipole moment alignment corresponds to an interfacial layer of only ∼0.3 nm thickness (one molecular layer).[55,56]

The slow proton transfer can also not result from the high concentration of bromide ions. To study the potential effect of bromide ions on the rate of proton transfer, we measured the proton hopping rate for different concentration of HBr in reverse micelles of two different sizes (see Figure S8) and in bulk solutions (see Figure S5). In neither case did we observe a significant effect of the concentration of HBr on the proton-transfer rate, which demonstrates that the slowing down of the proton transfer in water nanodroplets is not due to the high concentration of counterions.

Reverse micelles have also been used to study the effect of nanoconfinement on the reorientation dynamics of water molecules.[25,57−59] In these studies, it was found that nanoconfinement slows down the average reorientation of the water molecules, but not to the extent that we observe here for the proton transfer. For 7.4 nm nanodroplets, the reorientation time is expected to increase by ∼25% only, while the proton transfer time is observed to increase by a factor of 4.

The large difference in the effect of nanoconfinement on aqueous proton transfer in comparison to water molecular reorientation may be explained from the fact that proton transfer involves a much larger reorganization of the hydrogen-bond network than molecular reorientation.[49,60,61] Proton transfer involves an extended reorganization of the hydrogen-bond structure in which many water molecules and ions have to reorganize to allow for stabilization of the charges. This highly collective process will get frustrated if there is not enough space. In a recent molecular dynamics simulations study, it was found that the proton transfer in nonionic reverse micelles slows down primarily because the dynamics of the water hydrogen-bond network are significantly hindered.[62] An additional effect may be a long-range disruption of the hydrogen-bond network. Cringus et al.[39] found that intermolecular vibrational coupling between the water molecules in the core of AOT-stabilized water nanodroplets is strongly suppressed because of a disrupted hydrogen bond network. Car−Parrinello molecular dynamics simulations[63,64] show that water molecules that donate only one hydrogen bond or no hydrogen bond at all, cannot efficiently accept the proton due to their reduced basicity. As a result, the number of possible proton transfer pathways decreases and the average residence time of the proton at each water molecule increases.

In conclusion, we studied the vibrational and structural dynamics of proton hydration structures in bulk water and water nanodroplets that are stabilized with the cationic surfactant CTAB (cetyltrimethylammonium bromide) and hexanol, using polarization-resolved fs-IR spectroscopy. We observe that excitation of the OH-stretch vibrations of the hydrated proton at 2600 cm^{-1} results in long-living anisotropic absorption changes that largely decay as a result of proton hopping. For bulk acidic water proton hopping occurs with a time constant of 1.6 ps, in agreement with previous results. We observe the proton hopping to be ∼4 times slower for nanodroplets with a diameter of 7.4 nm and more than 10 times slower for nanodroplets with a diameter <4 nm. We thus find that nanoconfinement of liquid water strongly affects the rate of aqueous proton transfer, in contrast to other properties of water, like the reorientation of the water molecules. We hope that these results will stimulate new theoretical work to explain the exceptionally strong effect of 3D nanoconfinement on the rate of aqueous proton transfer.

METHODS

Sample Preparation. Nanodroplets were prepared by mixing *n*-hexane, 1-hexanol, cetyltrimethylammonium bromide (CTAB), water, and hydrobromic acid solution (48%) and stirring for 5 min. All the chemicals were purchased from Sigma-Aldrich. The concentrations of CTAB (0.11 M) and 1-hexanol (0.61 M) were the same for all microemulsions and yielded a ratio [hexanol]:[CTAB] = 3:1 in micellar phase.[65,66] Water and hydrobromic acid were added to obtain the desired w_0 = ([H_2O]+[HBr])/[CTAB] ratio and a concentration of HBr of 7 M in the nanodroplets. Without HBr this procedure yields nearly spherical monodisperse nanodroplets with a water pool diameter $d_w = 0.26 \times w_0$ (nm).[29,65,66] We estimate the size of the water nanodroplets with a particular w_0 to become 1.4 ± 0.2 times smaller when the water is replaced by an aqueous 7 M HBr solution, which implies that $d_w = 0.19 \times w_0$ (nm) (see Supporting Information, Figure S9). We also performed experiments with a lower HBr concentration (3 M). The results of these experiments are similar to those of the 7 M solution, but with a smaller signal-to-noise ratio (Figure S8). The samples were contained in a sample cell consisting of two 2 mm thick calcium fluoride windows separated by a 50−200 μm spacer. All the measurements were performed at 23 °C.

No unexpected or unusually high safety hazards were encountered.

Polarization-Resolved fs-IR Measurements. The two-color fs-IR experiments were performed with independently tunable pump and probe pulses. The details of the setup have been described before.[67] Briefly, 800 nm output (3.3 mJ) of a Ti:sapphire regenerative amplifier (Coherent) pumped two independent optical parametric amplification (OPA) processes followed by the mixing of signal and idler in a silver gallium disulfide crystal (AGS) produce mid-infrared excitation and detection pulses. The excitation pulses with an energy of 15 μJ, 100 fs pulse duration, and a full width at half-maximum (fwhm) of 160 cm^{-1}, were tuned to 2600 cm^{-1}. The detection pulses (0.3 μJ, 60 fs, 250 cm^{-1} fwhm) of tunable frequency were sent through a delay stage to introduce a variable time delay with respect to the pump. We used a single-color pump−probe setup for the anisotropy measurements at 2600 cm^{-1}. In this setup, a commercial OPA in combination with difference-frequency mixing of the signal and idler was pumped by an ytterbium-based laser (Light Conversion, 1030 nm, 0.4 mJ). This system produced mid-IR pulses with fwhm = 120 cm^{-1} and a duration of 200 fs, which were split into pulses of energies 4 μJ (excitation) and 0.2 μJ (detection) at the sample

https://dx.doi.org/10.1021/acscentsci.0c00340
ACS Cent. Sci. XXXX, XXX, XXX−XXX

position. In both setups every second excitation pulse was mechanically chopped. The excitation and detection beams were focused and overlapped in the sample. To correct for pulse-to-pulse fluctuations a reference beam was split off from the detection beam, and transmitted through the sample but not in overlap with the excitation beam. After the sample, the detection and reference beams were dispersed by a monochromator and measured with a mercury−cadmium−telluride (MCT) array detector, yielding the transient absorption spectrum as a function of the detection frequency. The absorption change spectrum was measured with both parallel and perpendicular polarization of the detection beam with respect to the polarization of the excitation beam. From these measurements we construct the isotropic signal $\Delta\alpha_{iso} = (\Delta\alpha_{\parallel} + 2\Delta\alpha_{\perp})/3$ and anisotropy $R = (\Delta\alpha_{\parallel} - \Delta\alpha_{\perp})/(\Delta\alpha_{\parallel} + 2\Delta\alpha_{\perp})$. For the anisotropy measurements, the accessible time window is determined by the decay rate of the isotropic signal. In our experiments, the anisotropy can be measured accurately up to 6−10 ps, depending on the size of the nanodroplet.

■ ASSOCIATED CONTENT

Supporting Information

The Supporting Information is available free of charge at https://pubs.acs.org/doi/10.1021/acscentsci.0c00340.

Transient spectra of nanodroplets of different sizes; additional plots on anisotropy dynamics; anisotropy dynamics of bulk HBr solutions; effect of hexanol molecules on the measured anisotropy; effect of the acid concentration on the anisotropy dynamics; vibrational dynamics of water molecules and size of the nanodroplets as a function of the ratio water:surfactant (PDF)

■ AUTHOR INFORMATION

Corresponding Author

Huib J. Bakker − *AMOLF, 1098 XG Amsterdam, The Netherlands;* orcid.org/0000-0003-1564-5314; Email: h.bakker@amolf.nl

Author

Oleksandr O. Sofronov − *AMOLF, 1098 XG Amsterdam, The Netherlands;* orcid.org/0000-0001-7744-6404

Complete contact information is available at: https://pubs.acs.org/10.1021/acscentsci.0c00340

Notes

The authors declare no competing financial interest.

■ ACKNOWLEDGMENTS

This work is part of the research program of The Netherlands Organization for Scientific Research (NWO) and was performed at the NWO research institute AMOLF. This project has received funding from the European Research Council (ERC) under the European Union's Horizon 2020 research and innovation program (grant agreement No 694386).

■ REFERENCES

(1) Pedersen, B. P.; Buch-Pedersen, M. J.; Preben Morth, J.; Palmgren, M. G.; Nissen, P. Crystal Structure of the Plasma Membrane Proton Pump. *Nature* **2007**, *450*, 1111−1114.

(2) Lozada-Hidalgo, M.; Zhang, S.; Hu, S.; Kravets, V. G.; Rodriguez, F. J.; Berdyugin, A.; Grigorenko, A.; Geim, A. K. Giant Photoeffect in Proton Transport through Graphene Membranes. *Nat. Nanotechnol.* **2018**, *13*, 300−303.

(3) Ramaswamy, P.; Wong, N. E.; Shimizu, G. K. H. MOFs as Proton Conductors − Challenges and Opportunities. *Chem. Soc. Rev.* **2014**, *43*, 5913−5932.

(4) Shimizu, G. K. H.; Taylor, J. M.; Kim, S. Proton Conduction with Metal-Organic Frameworks. *Science* **2013**, *341* (6144),.354.

(5) Agmon, N. The Grotthuss Mechanism. *Chem. Phys. Lett.* **1995**, *244*, 456−462.

(6) Marx, D.; Tuckerman, M. E.; Hutter, J.; Parrinello, M. The Nature of the Hydrated Excess Proton in Water. *Nature* **1999**, *397*, 601−604.

(7) Markovitch, O.; Chen, H.; Izvekov, S.; Paesani, F.; Voth, G. A.; Agmon, N. Special Pair Dance and Partner Selection: Elementary Steps in Proton Transport in Liquid Water. *J. Phys. Chem. B* **2008**, *112*, 9456−9466.

(8) Knight, C.; Voth, G. A. The Curious Case of the Hydrated Proton. *Acc. Chem. Res.* **2012**, *45*, 101−109.

(9) Biswas, R.; Tse, Y. L. S.; Tokmakoff, A.; Voth, G. A. Role of Presolvation and Anharmonicity in Aqueous Phase Hydrated Proton Solvation and Transport. *J. Phys. Chem. B* **2016**, *120*, 1793−1804.

(10) Kulig, W.; Agmon, N. A "clusters-in-Liquid" Method for Calculating Infrared Spectra Identifies the Proton-Transfer Mode in Acidic Aqueous Solutions. *Nat. Chem.* **2013**, *5*, 29−35.

(11) Daly, C. A.; Streacker, L. M.; Sun, Y.; Pattenaude, S. R.; Hassanali, A. A.; Petersen, P. B.; Corcelli, S. A.; Ben-Amotz, D. Decomposition of the Experimental Raman and Infrared Spectra of Acidic Water into Proton, Special Pair, and Counterion Contributions. *J. Phys. Chem. Lett.* **2017**, *8*, 5246−5252.

(12) Biswas, R.; Carpenter, W.; Fournier, J. A.; Voth, G. A.; Tokmakoff, A. IR Spectral Assignments for the Hydrated Excess Proton in Liquid Water. *J. Chem. Phys.* **2017**, *146*, 154507.

(13) Dahms, F.; Fingerhut, B. P.; Nibbering, E. T. J.; Pines, E.; Elsaesser, T. Large-Amplitude Transfer Motion of Hydrated Excess Protons Mapped by Ultrafast 2D IR Spectroscopy. *Science* **2017**, *357*, 491−495.

(14) Fournier, J. A.; Carpenter, W. B.; Lewis, N. H. C.; Tokmakoff, A. Broadband 2D IR Spectroscopy Reveals Dominant Asymmetric H5O2+ Proton Hydration Structures in Acid Solutions. *Nat. Chem.* **2018**, *10*, 932.

(15) Thompson, W. H. Solvation Dynamics and Proton Transfer in Nanoconfined Liquids. *Annu. Rev. Phys. Chem.* **2011**, *62*, 599−619.

(16) Muñoz-Santiburcio, D.; Marx, D. Chemistry in Nanoconfined Water. *Chem. Sci.* **2017**, *8*, 3444−3452.

(17) Spry, D. B.; Goun, A.; Glusac, K.; Moilanen, D. E.; Fayer, M. D. Proton Transport and the Water Environment in Nafion Fuel Cell Membranes and AOT Reverse Micelles. *J. Am. Chem. Soc.* **2007**, *129*, 8122−8130.

(18) Tielrooij, K. J.; Cox, M. J.; Bakker, H. J. Effect of Confinement on Proton-Transfer Reactions in Water Nanopools. *ChemPhysChem* **2009**, *10*, 245−251.

(19) Lawler, C.; Fayer, M. D. Proton Transfer in Ionic and Neutral Reverse Micelles. *J. Phys. Chem. B* **2015**, *119*, 6024−6034.

(20) Cohen, B.; Huppert, D.; Solntsev, K. M.; Tsfadia, Y.; Nachliel, E.; Gutman, M. Excited State Proton Transfer in Reverse Micelles. *J. Am. Chem. Soc.* **2002**, *124*, 7539−7547.

(21) Bardez, E.; Monnier, E.; Valeur, B. Dynamics of Excited-State Reactions in Reversed Micelles. 2. Proton Transfer Involving Various Fluorescent Probes According to Their Sites of Solubilization. *J. Phys. Chem.* **1985**, *89*, 5031−5036.

(22) Sedgwick, M.; Cole, R. L.; Rithner, C. D.; Crans, D. C.; Levinger, N. E. Correlating Proton Transfer Dynamics to Probe Location in Confined Environments. *J. Am. Chem. Soc.* **2012**, *134* (29), 11904−11907.

(23) Dokter, A. M.; Woutersen, S.; Bakker, H. J. Anomalous Slowing down of the Vibrational Relaxation of Liquid Water upon Nanoscale Confinement. *Phys. Rev. Lett.* **2005**, *94*, 4−7.

(24) Dokter, A. M.; Woutersen, S.; Bakker, H. J. Inhomogeneous Dynamics in Confined Water Nanodroplets. *Proc. Natl. Acad. Sci. U. S. A.* **2006**, *103*, 15355−15358.
(25) Moilanen, D. E.; Levinger, N. E.; Spry, D. B.; Fayer, M. D. Confinement or the Nature of the Interface? Dynamics of Nanoscopic Water. *J. Am. Chem. Soc.* **2007**, *129*, 14311−14318.
(26) Rabie, H. R.; Vera, J. H. Counterion Binding to Ionic Reverse Micellar Aggregates and Its Effect on Water Uptake. *J. Phys. Chem. B* **1997**, *101*, 10295−10302.
(27) Marques, B. S.; Nucci, N. V.; Dodevski, I.; Wang, K. W. C.; Athanasoula, E. A.; Jorge, C.; Wand, A. J. Measurement and Control of PH in the Aqueous Interior of Reverse Micelles. *J. Phys. Chem. B* **2014**, *118*, 2020−2031.
(28) Mukherjee, P.; Gupta, S.; Rafiq, S.; Yadav, R.; Jain, V. K.; Raval, J.; Sen, P. Ramping of pH Across the Water-Pool of a Reverse Micelle. *Langmuir* **2016**, *32*, 1693−1699.
(29) Fuglestad, B.; Gupta, K.; Wand, A. J.; Sharp, K. A. Water Loading Driven Size, Shape, and Composition of Cetyltrimethylammonium/Hexanol/Pentane Reverse Micelles. *J. Colloid Interface Sci.* **2019**, *540*, 207−217.
(30) Klíčová, L.; Šebej, P.; Štacko, P.; Filippov, S. K.; Bogomolova, A.; Padilla, M.; Klán, P. CTAB/Water/Chloroform Reverse Micelles: A Closed or Open Association Model? *Langmuir* **2012**, *28*, 15185−15192.
(31) Kim, J.; Schmitt, U. W.; Gruetzmacher, J. A.; Voth, G. A.; Scherer, N. E. The Vibrational Spectrum of the Hydrated Proton: Comparison of Experiment, Simulation, and Normal Mode Analysis. *J. Chem. Phys.* **2002**, *116*, 737−746.
(32) Xu, J.; Zhang, Y.; Voth, G. A. Infrared Spectrum of the Hydrated Proton in Water. *J. Phys. Chem. Lett.* **2011**, *2*, 81−86.
(33) Biswas, R.; Carpenter, W.; Fournier, J. A.; Voth, G. A.; Tokmakoff, A. IR Spectral Assignments for the Hydrated Excess Proton in Liquid Water. *J. Chem. Phys.* **2017**, *146*, 154507.
(34) Lock, A. J.; Woutersen, S.; Bakker, H. J. Ultrafast Energy Equilibration in Hydrogen-Bonded Liquids. *J. Phys. Chem. A* **2001**, *105*, 1238−1243.
(35) Ramasesha, K.; De Marco, L.; Mandal, A.; Tokmakoff, A. Water Vibrations Have Strongly Mixed Intra- and Intermolecular Character. *Nat. Chem.* **2013**, *5*, 935−940.
(36) De Marco, L.; Fournier, J. A.; Thämer, M.; Carpenter, W.; Tokmakoff, A. Anharmonic Exciton Dynamics and Energy Dissipation in Liquid Water from Two-Dimensional Infrared Spectroscopy. *J. Chem. Phys.* **2016**, *145*, 094501.
(37) Zischang, J.; Suhm, M. A. The OH Stretching Spectrum of Warm Water Clusters. *J. Chem. Phys.* **2014**, *140*, 064312.
(38) Seifert, G.; Patzlaff, T.; Graener, H. Size Dependent Ultrafast Cooling of Water Droplets in Microemulsions by Picosecond Infrared Spectroscopy. *Phys. Rev. Lett.* **2002**, *88*, 147402.
(39) Cringus, D.; Bakulin, A.; Lindner, J.; Vöhringer, P.; Pshenichnikov, M. S.; Wiersma, D. A. Ultrafast Energy Transfer in Water−AOT Reverse Micelles. *J. Phys. Chem. B* **2007**, *111*, 14193−14207.
(40) Sofronov, O. O.; Bakker, H. J. Vibrational Relaxation Dynamics of the Core and Outer Part of Proton-Hydration Clusters. *J. Phys. Chem. B* **2019**, *123*, 6222−6228.
(41) Meiboom, S. Nuclear Magnetic Resonance Study of the Proton Transfer in Water. *J. Chem. Phys.* **1961**, *34*, 375−388.
(42) Cringus, D.; Jansen, T. L. C.; Pshenichnikov, M. S.; Wiersma, D. A. Ultrafast Anisotropy Dynamics of Water Molecules Dissolved in Acetonitrile. *J. Chem. Phys.* **2007**, *127*, 084507.
(43) Liu, L.; Hunger, J.; Bakker, H. J. Energy Relaxation Dynamics of the Hydration Complex of Hydroxide. *J. Phys. Chem. A* **2011**, *115*, 14593−14598.
(44) Carpenter, W. B.; Fournier, J. A.; Lewis, N. H. C.; Tokmakoff, A. Picosecond Proton Transfer Kinetics in Water Revealed with Ultrafast IR Spectroscopy. *J. Phys. Chem. B* **2018**, *122*, 2792−2802.
(45) Laage, D.; Hynes, J. T. Reorientional Dynamics of Water Molecules in Anionic Hydration Shells. *Proc. Natl. Acad. Sci. U. S. A.* **2007**, *104*, 11167−11172.
(46) Laage, D.; Stirnemann, G.; Sterpone, F.; Rey, R.; Hynes, J. T. Reorientation and Allied Dynamics in Water and Aqueous Solutions. *Annu. Rev. Phys. Chem.* **2011**, *62*, 395−416.
(47) Berkelbach, T. C.; Lee, H.-S.; Tuckerman, M. E. Concerted Hydrogen-Bond Dynamics in the Transport Mechanism of the Hydrated Proton: A First-Principles Molecular Dynamics Study. *Phys. Rev. Lett.* **2009**, *103*, 238302.
(48) Maupin, C. M.; Aradi, B.; Voth, G. A. The Self-Consistent Charge Density Functional Tight Binding Method Applied to Liquid Water and the Hydrated Excess Proton: Benchmark Simulations. *J. Phys. Chem. B* **2010**, *114*, 6922−6931.
(49) van der Loop, T. H.; Ottosson, N.; Vad, T.; Sager, W. F. C.; Bakker, H. J.; Woutersen, S. Communication: Slow Proton-Charge Diffusion in Nanoconfined Water. *J. Chem. Phys.* **2017**, *146*, 131101.
(50) Tunuguntla, R. H.; Allen, F. I.; Kim, K.; Belliveau, A.; Noy, A. Ultrafast Proton Transport in Sub-1-Nm Diameter Carbon Nanotube Porins. *Nat. Nanotechnol.* **2016**, *11*, 639−644.
(51) Gopinadhan, K.; Hu, S.; Esfandiar, A.; Lozada-Hidalgo, M.; Wang, F. C.; Yang, Q.; Tyurnina, A. V.; Keerthi, A.; Radha, B.; Geim, A. K. Complete Steric Exclusion of Ions and Proton Transport through Confined Monolayer Water. *Science* **2019**, *363*, 145−148.
(52) Singh, P. C.; Nihonyanagi, S.; Yamaguchi, S.; Tahara, T. Interfacial Water in the Vicinity of a Positively Charged Interface Studied by Steady-State and Time-Resolved Heterodyne-Detected Vibrational Sum Frequency Generation. *J. Chem. Phys.* **2014**, *141*, 18C527.
(53) Nguyen, K. T.; Nguyen, A. V. Suppressing Interfacial Water Signals to Assist the Peak Assignment of the N+-H Stretching Mode in Sum Frequency Generation Vibrational Spectroscopy. *Phys. Chem. Chem. Phys.* **2015**, *17*, 28534−28538.
(54) Nguyen, K. T.; Nguyen, A. V.; Evans, G. M. Interfacial Water Structure at Surfactant Concentrations below and above the Critical Micelle Concentration as Revealed by Sum Frequency Generation Vibrational Spectroscopy. *J. Phys. Chem. C* **2015**, *119*, 15477−15481.
(55) Agazzi, F. M.; Correa, N. M.; Rodriguez, J. Molecular Dynamics Simulation of Water/BHDC Cationic Reverse Micelles. Structural Characterization, Dynamical Properties, and Influence of Solvent on Intermicellar Interactions. *Langmuir* **2014**, *30*, 9643−9653.
(56) Chowdhary, J.; Ladanyi, B. M. Molecular Simulation Study of Water Mobility in Aerosol-OT Reverse Micelles. *J. Phys. Chem. A* **2011**, *115*, 6306−6316.
(57) Dokter, A. M.; Woutersen, S.; Bakker, H. J. Ultrafast Dynamics of Water in Cationic Micelles. *J. Chem. Phys.* **2007**, *126*, 124507.
(58) Van der Loop, T. H.; Panman, M. R.; Lotze, S.; Zhang, J.; Vad, T.; Bakker, H. J.; Sager, W. F.; Woutersen, S. Structure and Dynamics of Water in Nonionic Reverse Micelles: A Combined Time-Resolved Infrared and Small Angle X-Ray Scattering Study. *J. Chem. Phys.* **2012**, *137*, 044503.
(59) van der Loop, T. H.; Ottosson, N.; Lotze, S.; Kentzinger, E.; Vad, T.; Sager, W. F. C.; Bakker, H. J.; Woutersen, S. Structure and Dynamics of Water in Nanoscopic Spheres and Tubes. *J. Chem. Phys.* **2014**, *141*, 18C535.
(60) Tielrooij, K. J.; Timmer, R. L. A.; Bakker, H. J.; Bonn, M. Structure Dynamics of the Proton in Liquid Water Probed with Terahertz Time-Domain Spectroscopy. *Phys. Rev. Lett.* **2009**, *102* (19), 1−4.
(61) Lapid, H.; Agmon, N.; Petersen, M. K.; Voth, G. A. A Bond-Order Analysis of the Mechanism for Hydrated Proton Mobility in Liquid Water. *J. Chem. Phys.* **2005**, *122* (1), 014506.
(62) Li, Z.; Voth, G. A. Interfacial Solvation and Slow Transport of Hydrated Excess Protons in Non-Ionic Reverse Micelles. *Phys. Chem. Chem. Phys.* **2020**, *22*, 10753.
(63) Bankura, A.; Chandra, A. Proton Transfer through Hydrogen Bonds in Two-Dimensional Water Layers: A Theoretical Study Based on Ab Initio and Quantum-Classical Simulations. *J. Chem. Phys.* **2015**, *142*, 044701.
(64) Dellago, C.; Naor, M. M.; Hummer, G. Proton Transport through Water-Filled Carbon Nanotubes. *Phys. Rev. Lett.* **2003**, *90*, 105902.

https://dx.doi.org/10.1021/acscentsci.0c00340
ACS Cent. Sci. XXXX, XXX, XXX−XXX

(65) Palazzo, G.; Lopez, F.; Giustini, M.; Colafemmina, G.; Ceglie, A. Role of the Cosurfactant in the CTAB/Water/n-Pentanol/n-Hexane Water-in-Oil Microemulsion. 1. Pentanol Effect on the Microstructure. *J. Phys. Chem. B* **2003**, *107*, 1924−1931.
(66) Mills, A. J.; Britton, M. M. NMR Study of the Influence of N-Alkanol Co-Surfactants on Reverse Micelles in Quaternary Micro-emulsions of Cetyltrimethylammonium Bromide (CTAB). *Magn. Reson. Chem.* **2017**, *55*, 425−432.
(67) Sofronov, O. O.; Bakker, H. J. Energy Relaxation and Structural Dynamics of Protons in Water/DMSO Mixtures. *J. Phys. Chem. B* **2018**, *122*, 10005−10013.

https://dx.doi.org/10.1021/acscentsci.0c00340
ACS Cent. Sci. XXXX, XXX, XXX−XXX